



NIH Public Access

Author Manuscript

Proteins. Author manuscript; available in PMC 2013 June 01.

Published in final edited form as:
Proteins. 2012 June ; 80(6): 1582–1597. doi:10.1002/prot.24052.

Structural Transitions and Oligomerization along Polyalanine Fibril Formation Pathways from Computer Simulations

Erin M. Phelps* and **Carol K. Hall***

*Department of Chemical and Biomolecular Engineering, North Carolina State University, Raleigh, NC 27695, USA

Abstract

The results of a computer simulation study of the aggregation kinetics of a large system of model peptides with particular focus on the formation of intermediates are presented. Discontinuous molecular dynamic simulations were used in combination with our intermediate-resolution protein model, PRIME, to simulate the aggregation of a system of 192 polyalanine (KA₁₄K) peptides at a concentration of 5mM and reduced temperature of T* = 0.13 starting from a random configuration and ending in the assembly of a fibrillar structure. The population of various structures, including free monomers, beta sheets, amorphous aggregates, hybrid aggregates, and fibrils, and the transitions between the structures were tracked over the course of thirty independent simulations and averaged together. The aggregation pathway for this system starts with the association of free monomers into small amorphous aggregates that then grow to moderate size by incorporating other free monomers or merging with other small amorphous aggregates. These then rearrange into either small beta sheets or hybrid aggregates formed by association between unstructured chains and beta sheets, both of which grow in size by adding free monomer chains or other small aggregates, one at a time. Fibrillar structures are formed initially either by the stacking of beta sheets, rearrangement of hybrid aggregates or association between beta sheets and hybrid aggregates. They grow by the addition of beta sheets, hybrid aggregates and other small fibrillar structures. The rearrangement of amorphous aggregates into beta sheets is a critical and necessary step in the fibril formation pathway.

Keywords

amyloid; protein aggregation; fibril formation pathway; computer simulations

Introduction

Protein aggregation is widely studied in the scientific and medical communities due to its connection to human neurodegenerative diseases such as Alzheimer's, Parkinson's, Huntington's, Creutzfeld-Jakob, and the prion diseases.^{1–7} Each of these diseases is characterized by the presence of protein deposits composed of ordered protein aggregates known as amyloid fibrils. Fibrils are long, straight, and un-branched structures containing several proto-filaments, each of which exhibits "cross beta structure," – ribbon-like layers of large beta sheets whose strands run perpendicular to the fibril axis.^{1, 8–10} Although it was originally believed that fibrillar aggregates were responsible for cell disruption and death (the so-called amyloid cascade hypothesis), more recent work has suggested that the precursors to fibril formation, particularly small intermediate oligomers, are the toxic

Corresponding Author: Dr. Carol K. Hall, Department of Chemical and Biomolecular Engineering, North Carolina State University, Raleigh, NC 27695, USA. Phone: (919) 515 – 3571, Fax: (919) 515 – 3465, hall@ncsu.edu.

species and that fibrils might just be nature's way of sequestering bad actors.^{11–16} If the early-oligomers-as-toxic-species hypothesis is correct, it becomes critically important to determine the pathway that a protein takes in going from a natively-folded or unfolded state to the toxic state and beyond in order to discover the best way to interfere with and/or inhibit the toxic events.

The general consensus in the protein aggregation community concerning the sequence of events along the fibril formation pathway is the following. Partially or totally unfolded monomer peptides aggregate into small intermediate oligomers that are unstable and transient in nature. These oligomers rearrange into an organized conformation containing the cross beta structure and then associate into proto-filaments and finally into full fibrils.^{11, 17–19} Recent studies have suggested that toxic intermediate oligomers may form as a side reaction to fibril formation, which means that it might be possible to prevent the formation of the toxic intermediate species without disrupting the overall fibril formation process.^{20–23}

The goal of this work is to provide insights into the pathway that proteins follow as they evolve from monomers through intermediates to proto-filaments. The method used is molecular-level computer simulations, which offers the opportunity to observe the formation of small intermediates directly (albeit imprecisely) as the position, trajectories, and interactions of every atom are monitored during the course of the simulation.^{24–28} This molecular level description of the aggregation process provides a useful complement to experimental studies, which have difficulty tracking the formation of smaller intermediate structures because of their unstable and transient nature. This means that most of the information about aggregation kinetics gleaned from analyses of experimental data is indirect or inferred; typically the only data recorded are the concentrations of free monomers and fully formed fibrils, *i.e.* the starting and ending points of the proposed pathways. There are many different hypotheses in the literature concerning the number and type of intermediates along the aggregation pathway, but these cannot be confirmed directly due to the difficulty of measuring the populations of the various intermediates over time.^{29–36} Most of the proposed aggregation pathways progress from free monomers to small unstable oligomeric species to protofilaments composed of elongated beta sheets to fully formed fibrils.^{11, 37, 38}

One way to extract information on aggregation pathways from experimental kinetics data is to assume a reaction mechanism, derive the associated set of reaction equations and then fit the various rate constants to population data.^{19, 39–42} The most popular reaction mechanism appearing in the literature is nucleated polymerization in which monomers slowly and reversibly come together to form small, energetically unstable intermediates that serve as a nucleus. Once the nucleus is formed monomers quickly and irreversibly attach themselves to the aggregate which continues to grow, eventually forming proto-filaments that then laterally associate into fibrils.^{19, 42–44} Lomakin *et al.* showed that nucleus formation and elongation of fibrils was dependent upon the initial concentration of monomers in the system and the tendency to form micelles.⁴² Another oft-assumed reaction mechanism is monomer-directed conversion in which a monomer undergoes a structural transition from a native state to a pre-fibrillar state and then influences other native state monomers to undergo the same transition, forming an intermediate fibrillar structure that eventually grows into a fibril.^{45, 46} A third proposed mechanism in the literature is templated assembly, in which a native state monomer binds to a pre-existing fibrillar structure and then undergoes a structural transition to a fibrillar conformation.^{47–49} It is difficult to decide which of the proposed mechanisms is better or more accurate than the others since there is limited information available about the intermediate structures, as discussed in detail by Bernacki and Murphy.⁵⁰

Another way to extract information on aggregation pathways from kinetics data is to prevent specific reactions from occurring by using targeted inhibitors or other constraints to block formation of the intermediates that are expected to occur along that pathway. Examples of the types of structures that might be inhibited include small pre-fibrillar structures, fully formed fibrils, and certain types of oligomers.^{22, 23, 46, 51} In this way, one determines which of the small intermediate aggregates that are formed during the fibrillization process are truly necessary steps in the kinetic pathway, and which are side reactions that could be minimized. Knowing whether the toxic intermediates are necessary on-path species, or competitive side-path species helps us to come up with specific targets for drugs or other treatment options.^{13, 20, 22, 23} Glabe and coworkers have applied this approach to A β peptides. The intermediates that were formed were classified into three different types: a stable intermediate, an intermediate that is a stepping stone to fibril formation, and an intermediate that rearranges into a spherical oligomer which can but does not easily proceed to form fibrils. Spherical oligomers were found to be much more toxic than either of the other two types of intermediates.^{13, 22, 23}

One part of the kinetic pathway that has received a fair amount of attention is the collapse of a single peptide into an amorphous globular state and its subsequent rearrangement to form cross-beta structure. Using computer simulations Pappu and coworkers found that the early stages of polyglutamine aggregation are characterized by the collapse of single peptides into amorphous globules that then associate with other collapsed peptides.⁵²⁻⁵⁴ Lindquist and coworkers showed that long yeast prion sequences initially collapse into amorphous domains with hydrophobic (head) or hydrophilic (tail) content, much like micelles. The conformations of the peptides within the head region of the collapsed amorphous domain become more ordered with time, initiating the formation of an amyloid structure. This amyloid structure then propagates in both the head and tail directions by influencing other collapsed peptides to adopt the amyloid structure.⁵⁵⁻⁵⁷ Ding *et al.* first investigated the formation of dimers and then the aggregation of eight Src SH3 domain proteins using computer simulations and found that after the monomeric form of the peptide partially unfolded there was competition between folding back to the native state and aggregation with a neighboring peptide that had also partially unfolded. This aggregate could then continue to add partially unfolded monomeric peptides.⁵⁸ Most investigations of the fibril formation pathway indicate that amorphous aggregates play an important role in the transition from monomers to the more ordered intermediates that grow into fully-formed fibrils, whether as a necessary step in the fibrillization pathway or as a side reaction that produces toxic species. If this amorphous-aggregate-to-ordered-structure transition could be better quantified, it could lead to new insights into the aggregation pathway and the pathogenic processes underlying the amyloid diseases.

In this paper we analyze the kinetics from computer simulations of the spontaneous aggregation of a large system of polyalanine (KA₁₄K) chains in order to determine the types and quantities of intermediate species that appear during the fibril formation process. Polyalanine was chosen as the model peptide because it is known to form fibrils *in vitro* under slightly - denatured concentrated conditions.⁵⁹ Previous simulations performed in our group on a system of 48 polyalanine chains using a combination of discontinuous molecular dynamics (DMD) simulations and our intermediate resolution protein model (PRIME) resulted in the spontaneous formation of fibrillar structures (protofilaments) whose physical characteristics (including inter- and intra-sheet distances) and trends (alpha helix to beta sheet transition) with temperature were in reasonably good agreement with experimental results.⁶⁰⁻⁶³ In this paper we perform new simulations on a much larger system (192 chains) in order to get detailed information on the kinetics of protein aggregation with particular focus on the formation of intermediate structures, including amorphous aggregates, along the aggregation pathway. Each simulation was started in a random configuration of random

coils at a concentration of 5mM and a reduced temperature of $T^*=0.13$, a temperature that was shown to produce a large population of well-ordered fibrillar structures at this concentration in previous studies. The simulations were run until approximately 90% of the chains had aggregated into some form of ordered structure, most often a large fibrillar structure. The position and interaction partners of each chain were recorded at regular time intervals (one unit of simulation time), leading to the classification of each chain at each time as being in a particular “aggregation state”: free monomer, amorphous aggregate containing w chains, hybrid aggregate containing x chains, beta sheet containing y chains, or fibril (proto-filament) containing n sheets with z chains. The sequence of aggregation states occupied by each chain over the course of the simulations was used to analyze the aggregation process, and summarized in terms of population data (fraction of peptides in each state) and transitions from one state to another as a function of reduced time.

Highlights of our results include the following. The general picture of the aggregation pathway for large systems of KA₁₄K peptides that has emerged from these simulations is the following. Initially, individual free monomer chains associate together into small and intermediate-sized amorphous aggregates that then grow to moderate size by incorporating other free monomers or merging with other small amorphous aggregates. These then rearrange into either small beta sheets or hybrid aggregates formed by association between unstructured chains and beta sheets, both of which grow in size by adding free monomer chains or other small aggregates, one at a time. Fibrillar structures are formed initially either by the stacking of beta sheets, rearrangement of hybrid aggregates or association between beta sheets and hybrid aggregates. They grow by the addition of beta sheets, hybrid aggregates and other small fibrillar structures. The most common sizes of the initial amorphous aggregates, hybrid aggregates, and beta sheets are between two and seven chains, while the size of the fibrils grows from initially less than ten chains to around 150 chains in the final structure. Few free monomers, amorphous aggregates, or independent beta sheets remain at the end of the simulation. The amorphous aggregates and small beta sheets that form during the simulation are all necessary steps along the aggregation pathway. Beta sheets start to appear in the simulation at about the same time as the peak of the amorphous aggregate population; similarly fibrils start to appear at about the same time as the peak in the beta sheet population, indicating that there is a natural progression from free monomers to amorphous aggregates to beta sheets and/or hybrid aggregates to fibrils.

Analysis of the transitions from one aggregation state to another shows that the amorphous aggregates reorganize into beta sheets twice as often as the beta sheets collapse into amorphous aggregates. This leads to the conclusion that the restructuring of amorphous aggregates into beta sheets plays a key role in the fibrillization mechanism; this is hypothesized to be a nucleation step for the prion Sup35,⁵⁷ for A β ₁₆₋₂₂,⁶⁴ and for generic protein sequence¹⁸. The small amorphous aggregates are unstable under the simulation conditions; by the end many of them wind up interacting with the large fibril and subsequently rearranging to form cross- β structures that add on to the fibril. The small beta sheets that are formed from the rearrangement of the amorphous aggregates are themselves unstable due to the exposed hydrophobic side chains, and therefore quickly associate into small fibrillar structures that grow over the course of the simulation until the final protofilament-like structure is formed. Two-sheet fibrils form both by the association of two beta sheets or by the association of a restructuring amorphous or hybrid aggregates with a single beta sheet, which indicates that beta sheets can influence amorphous aggregate structure and propagate the cross- β conformation. The instability of the small oligomers and their subsequent growth into large fibrillar structures suggests nucleation behavior and is consistent with proposed fibril formation pathway results published in the literature for A β ₁₋₄₀^{19, 22} and in a mathematical model published by Powers.⁴³ The fibrillization mechanisms seen in these simulations are more complicated than the polymerization

mechanisms (nucleated polymerization, nucleated conformational conversion, and templated assembly) traditionally used to describe amyloid fibrillization.

Materials and Methods

We performed computer simulations of a system of 192 chains comprised of the peptide KA₁₄K each starting from a different initial random configuration. The peptide geometry and force field were modeled using PRIME, an intermediate resolution protein model developed in the Hall group.^{60–63, 65, 66} Each peptide residue is represented by four spheres; one for the carbonyl carbon and its associated oxygen atom, one for the amide nitrogen and its associated hydrogen atom, one for the alpha carbon and its associated hydrogen atom, and one for the side chain atoms. Figure 1 shows a schematic of the PRIME protein geometry. Each united atom is attached to the next with a covalent bond of a realistic length taken from the literature. The geometry of the peptide chain is maintained by imposing pseudo-bonds between the united atom spheres that restrict the backbone bond angles to realistic values, maintain the peptide bond in the *trans* conformation and ensure the L-isomerization of the side chain.

Solvent is modeled implicitly by including hydrophobic interactions between non-polar side chains. All interactions in the system are modeled as either hard sphere, square well, or square shoulder potentials. Excluded volume for each sphere is modeled by a hard sphere potential with a realistic diameter. The lengths of all covalent bonds and pseudo-bonds are allowed to fluctuate within a tolerance of 2.375% by setting up hard sphere repulsions any time the length of the bond attempts to move outside of the range of $\lambda(1 - \delta)$ to $\lambda(1 + \delta)$ where λ is the ideal length of the bond and δ is the tolerance.

PRIME accounts for the two most basic types of inter- and intra-peptide interactions: hydrogen bonding and hydrophobic interactions. Hydrogen bonding is modeled as a square well attraction of depth ϵ_{HB} between the carbonyl and amide spheres on the same and neighboring chains when certain criteria are met as described in a previous article.⁶⁷ Hydrophobic interactions are captured in this model by a square well attraction of depth ϵ_{HP} and width $1.5\sigma_R$ between hydrophobic side chain united atoms (where σ_R is the side chain sphere diameter) provided that they are on separate chains or at least three residues apart on the same chain. The reduced simulation temperature is scaled with the hydrogen bond strength, $T^* = k_B T / \epsilon_{HB}$, where k_B is Boltzmann's constant; in this paper $T^* = 0.13$. The relative strength of the hydrophobic attraction and hydrogen bond strength, $R = \epsilon_{HP} / \epsilon_{HB}$ is set here to $R = 0.10$ as in our previous simulations of polyalanine.^{60–63, 67}

The simulations were performed using discontinuous molecular dynamics (DMD), an alternative to traditional molecular dynamics that is applicable to systems modeled using a combination of discontinuous potentials, i.e. hard sphere and square-well potentials. Unlike continuous potentials, such as the Lennard-Jones potential, discontinuous potentials exert forces only when particles collide, enabling the exact (as opposed to numerical) solution of the collision dynamics. This imparts great speed to the algorithm, allowing sampling of longer time scales and larger systems than in traditional molecular dynamics. DMD proceeds in the following manner. Particles are initially placed in a random configuration consistent with excluded volume and angular constraints. Initial velocities are assigned based on a Maxwell-Boltzmann distribution about the simulation temperature. The time until the first event (first discontinuity in a potential) is calculated, the particles are advanced along their trajectories toward that event, the new velocities of the colliding particles are calculated and assigned, and the process starts all over again. Types of events that occur during the simulation are excluded volume events when spheres collide, bond events when the distance between two bonded spheres reaches a limit, and square well or square shoulder

events when two spheres enter (capture), unsuccessfully attempt to leave (bounce), or successfully leave a square well attraction or square shoulder repulsion (dissociation) interaction.^{68–71}

All of the simulations were carried out in the canonical ensemble, where the number of particles, the temperature, and the volume of the simulation are held constant. The box length of the cubic simulation cell was set at 399.6 Å in order to create the desired concentration of 5mM for the 192 KA₁₄K peptides. Periodic boundary conditions were implemented to eliminate any artifacts due to the simulation box walls. The temperature was held constant using the Andersen thermostat, which utilizes ghost collisions with random particles in the system to maintain the Maxwell-Boltzmann velocity distribution about the desired system temperature.⁷² The simulation time was measured in terms of a reduced time units, $t^* = t / (\sigma \sqrt{k_B T / m})$, where t is the simulation time and σ and m are the average sphere diameter and mass respectively. Since DMD is driven by collisions, not pre-determined time steps, and there are no solvent particles, it is difficult to relate the reduced time to a real time scale. All results will be given in terms of reduced simulation time.

Thirty simulation runs were performed starting from a different random initial configuration and the results were averaged together. Over the course of each simulation the populations of different structures such as free monomer chains, beta sheets of specific sizes, amorphous aggregates of specific sizes, hybrid aggregates of specific sizes, and fibrils were recorded as a function of time.

Each peptide chain is classified into one of five possible structures (free monomer – M, amorphous aggregate – A, hybrid aggregate – H, beta sheet – B, or fibril – F) by analyzing the number and type of interactions that the atoms in the peptide chain have with other chains in the system. Figure 2 shows snapshots of four of the classes of structures. A free monomer is defined to be any chain that has no interaction, either hydrophobic or hydrogen bonding, with another chain in the system. A beta sheet is defined to be a set of two or more peptide chains that have at least eight hydrogen bonds (half of the chain length) between each pair of neighboring chains in the sheet. (Hydrophobic contacts are not considered when determining beta sheets.) Fibrils are defined to be beta sheets with at least three hydrophobic interactions between two different pairs of chains in the beta sheets, for a total of at least six hydrophobic contacts. Amorphous aggregates are defined to be a set of chains that have hydrophobic contacts or hydrogen bonds between them in which none of the chains in the aggregate are within a beta sheet or a fibril. Hybrid aggregates are defined to be a set of chains that have hydrophobic contacts or hydrogen bonds between them in which some but not all of the chains are within a beta sheet or a fibril. A chain that is classified as being in a hybrid aggregate state is unstructured but has hydrophobic contacts or hydrogen bonds with chains that are either in a beta sheet or fibrillar state. (The structured chains in the hybrid aggregate are classified as being in the beta sheet or fibrillar state, whichever is applicable.) The hybrid aggregate is introduced to account for aggregates that are not completely amorphous. It is a useful construct for examining the transition from amorphous aggregates to more ordered structures.

Over the course of the simulation the populations for free monomers (M), beta sheets containing two (B₂), three (B₃), four (B₄), five (B₅), six (B₆), seven (B₇), and more than seven chains (B_S), fibrils containing two (F₂), three (F₃), four (F₄), five (F₅), six (F₆), and more than six beta sheets (F_S), amorphous aggregates containing two (A₂), three (A₃), four (A₄), five (A₅), six (A₆), seven (A₇), and more than seven (A_S) chains, and hybrid aggregates containing two (H₂), three (H₃), four (H₄), five (H₅), six (H₆), seven (H₇), and more than seven (H_S) chains were recorded as a function of simulation time. In order to prevent double counting, chains are classified according to the most ordered structure they

belong to, so that for example a chain classified as being part of a fibril would not also be classified as being part of a beta sheet.

In addition to recording population data, each individual chain is given an identification label at each time step that indicates the highest order aggregation state to which it belongs. Free monomer chains are given an identification label that signifies that they are not interacting with any other chains at that specific simulation time. Chains in a beta sheet are given an identification label that indicates how many chains are in that specific beta sheet. Chains within a fibril are given an identification label that indicates how many sheets are in the fibril, how many total chains are in the fibril, and how many chains are in the individual beta sheet that contains that particular chain. Chains within an amorphous aggregate are given an identification label that indicates how many chains are in that specific aggregate. Chains within a hybrid aggregate are given an identification label that indicates how many chains are in the overall aggregate; this total number of chains for the aggregate can include both the chains classified as hybrid and the chains found in ordered structures such as beta sheets or fibrils with which the hybrid chains are interacting. All of this information allows us to track the progress of individual chains and make determinations as to how particular intermediate structures form and change throughout the simulation. By keeping track of the changes in chain identification labels as a function of time, it is possible to determine how certain intermediates form and dissociate or grow into larger structures.

Results

Population of Various Structures Versus Time

Thirty simulations of 192 peptide chains with sequence KA₁₄K starting from a random coil configuration at a reduced temperature of T* = 0.13 and a concentration of 5mM were performed and the results were averaged together. Figure 3 displays the snapshots at various times from one typical simulation to illustrate the fibrillization pathway. At time t* = 0, the system is a configuration of random coils; the peptides are not interacting with each other. At time t* = 5 the system shows the formation of small amorphous aggregates. As the simulation progresses, these amorphous aggregates rearrange into beta sheets, shown at t* = 16, which then associate into small fibrils consisting of two sheets and between eight to ten chains (see t* = 21). These fibrils then continue to grow (see t* = 32) and add beta sheets throughout the simulation until most of the peptide chains organize into a large structure consisting of about 165 chains, shown at t* = 106. At this point in the simulation the peptides are rearranging within the large structure in order to minimize the free energy of the system. Since we are interested in the formation of the fibril and not in its restructuring, we stopped the simulation at t* = 106. At the end of this particular simulation, there is one large fibril with 165 chains; the remaining peptides are either free monomers or are attached to the fibril in a hybrid aggregate state.

Figure 4 contains population data averaged over the thirty simulations as a function of reduced simulation time. The notation here [A₂, A_j (j > 2), H_k (k = 2), B_k (k = 2), and F_n (n = 2)] and in subsequent figures is the following: A₂ represents the population of 2-chain amorphous aggregates, A_j represents the population of amorphous aggregates containing more than two chains, H_k and B_k represent the populations of hybrid aggregates and beta sheets, respectively, containing two or more chains, and F_n represents the population of fibrils containing two or more beta sheets. When no subscript is given the population refers to the total number of chains in that type of aggregate. This notation is used in all subsequent figures unless otherwise noted. Figure 4a shows the percentage of peptide chains in each structure class (free monomer, amorphous aggregate, hybrid aggregate, beta sheet, and fibril). Figures 4b and 4c show the number of amorphous aggregates and beta sheets containing a specific number of chains. Figure 4d shows the number of fibrils containing a

specific number of beta sheets. Populations less than one in Figures 4b, 4c, and 4d are possible because these results are an average over thirty different simulations. That means that if fifteen of the simulations exhibit a single five-chain beta sheet at a particular time and the other fifteen don't, at that time the population of a five chain beta sheet (B_5) will register as 0.5.

As Figure 4a indicates, the system starts with free monomer at time $t^* = 0$ and rapidly forms amorphous aggregates whose population peaks and then declines; this is accompanied by the slow formation of beta sheets and hybrid aggregates, and then the appearance of fibrils once the beta sheet population peaks. The fibrils grow steadily as the populations of all other aggregation states diminish until the system reaches a point where approximately 90% of the chains are in a fibril and the system seems to stabilize. Throughout the simulation there are always more chains in either amorphous or hybrid aggregates than in individual beta sheets, which indicates that the single (isolated) beta sheet conformation is less favorable than the amorphously aggregated conformation. Instead of remaining isolated, the single beta sheets stack to form fibrils which are then stabilized by the hydrophobic interactions. This makes sense because amorphous aggregates can collapse and protect the hydrophobic side chains, while individual beta sheets leave all of the side chains exposed to solvent.

Examination of Figures 4b–4d gives a more detailed picture of the aggregation pathway than that suggested by the overall population data shown in Figure 4a. Figure 4b shows that the amorphous aggregate structures that form in the beginning of the simulation are most likely to be small; over 20 amorphous aggregates contain two chains (A_2). All of the amorphous aggregate populations exhibit a peak before $t^* = 25$, and as the size of the amorphous aggregate increases, its population decreases. The aggregation state A_8 refers to all of the amorphous aggregates with more than seven chains and so its peak exceeds that of the largest specific size aggregate. As we saw in Figure 4a the beta sheet population begins to grow as the amorphous aggregate population begins to diminish. Figure 4c shows that the dimer population (B_2) peaks around $t^* = 20$, followed quickly by trimers (B_3) at $t^* = 25$ and tetramers (B_4) at $t^* = 30$. Larger beta sheets containing five or more chains (B_5 , B_6 , B_7 , and B_8) do appear in the simulations, but they do not do so at the same time in every simulation, so their populations remain at or below one over the course of the simulation. At approximately $t^* = 25$ the total beta sheet population goes through a peak (seen in Figure 4a), and thereafter individual beta sheets begin to disappear (Figure 4b) as fibrils begin to form and grow. Figure 4d shows that multiple small fibrils of either two (F_2) or three (F_3) sheets appear first in the simulations. These fibrils then slowly combine or add new beta sheets until they fall into the large fibril category (F_8) with more than six sheets. At the end of the thirty simulation runs, fifteen of the systems had two large fibrils attempting to interact and form one even larger fibril, and the other fifteen systems had one large fibril structure.

Structural Transitions Versus Time

The information that we record on the aggregation state of each chain over the course of the simulations can be used to learn more about how the different types of aggregates form, grow and diminish as a function of time. The transitions from one type of aggregation state to another have been broken down into five categories, those that start from or result in a free monomer M (Figure 5), those that start from or result in an amorphous aggregate A (Figure 6), those that start from or result in a hybrid aggregate H (Figure 7), those that start from or result in a beta sheet B (Figure 8), and those that start from or result in a fibril F (Figure 9). The y-axis in each figure, percentage of a particular type of transition, is the number of transitions of that particular type divided by the total number of peptide chains that are in the same starting (or ending) overall aggregation state. So for example at any one time, the percentages of transitions that result in an amorphous aggregate from free

monomers ($M \rightarrow A$), from amorphous aggregates ($A \rightarrow A$), from hybrid aggregates ($H \rightarrow A$), from beta sheets ($B \rightarrow A$), and from fibrils ($F \rightarrow A$) add up to 100%. This means that direct comparison of percentage values from one figure to another is not meaningful since the total number of chains is not the same for each category. Comparison of percentage values between graphs in separate columns of the same figure (to and from a particular state) is possible because the difference in the total number of chains in a category does not change significantly from one time point to the next and so the denominators for each set of transitions are nearly equal. Transitions where no change in identity occurred, such as a free monomer remaining a free monomer, are recorded and included in the normalization, but not shown for clarity.

Figure 5 shows the percentage of transitions that start from or end up in the free monomer state as a function of time. Before describing the results in Figure 5, it is important to point out that the monomeric peptides in these simulations behave largely as random coils, showing little tendency to form alpha helices. This is because the simulations are conducted at a temperature that is above the folding temperature of $T^* = 0.11$.⁶⁷ A very small number of alpha-helical hydrogen bonds form at the beginning of the simulation; this number decreases slightly as the simulations progress. No stable alpha-helices are formed at any point in the simulations. Figure 5a shows the transitions from free monomer to aggregation states for amorphous and hybrid aggregates, beta sheets and fibrils. It is apparent that free monomers associate almost exclusively to form amorphous or hybrid aggregates. We do see free monomers adding on to existing beta sheets or fibrils, but these transitions do not occur often; those that do are hidden in the noise since the results are averaged over thirty simulations. Figure 5b shows transitions that result in free monomer starting from A_2 , A_j , and H_k . The percentages of transitions to free monomer from beta sheets and fibrils are very small and so are not included in this figure. Most of the transitions that produce a free monomer result from an amorphous aggregate losing a chain, either through dissolution of an amorphous aggregate with two chains (A_2), or loss of a single chain from a larger amorphous aggregate (A_j) at early time points. Events in which a single chain breaks off from an existing beta sheet or a fibril do not occur with any regularity, so the few times this happens become noise in the average. Since the individual simulations do show that peptides can release from amorphous aggregates, hybrid aggregates, beta sheets, and fibrils, it indicates that the aggregation pathway is reversible. At this particular temperature however it is more energetically favorable to stay in an ordered structure, so the number of transitions to free monomer decreases as the large fibril structure forms at long times. This is consistent with the population data that shows that the number of free monomers declines to almost zero at the end of the simulation.

Examination of Figure 5 also gives us information about the formation of amorphous aggregates. At early times (before the amorphous aggregate population peak at $t^* = 15$) the vast majority of transitions to amorphous aggregates come from free monomers due to the absence of any other types of structures. After $t^* = 15$ the percentage of monomers forming amorphous aggregates slowly tapers off due to the diminishing monomer population and new opportunities for monomers to add to beta sheets or hybrid aggregates. At the end of the simulation there are few free monomers and few amorphous aggregates, so the percentage of transitions involving a free monomer adding on to an amorphous aggregate goes to zero.

Figure 6 shows the percentage of the transitions that start from or end up in an amorphous aggregate including: the percentage of transitions that start from (a) hybrid aggregates, and (b) beta sheets, and the percentage that end up as (c) hybrid aggregates, and (d) beta sheets as a function of time. We do not include plots of the transitions between amorphous aggregates and free monomers, other amorphous aggregates, or fibrils because these would not provide additional information beyond what is presented in other figures in the paper. In

these figures $m > 1$, so for example $H_{k+m} \rightarrow A_k$ refers to the population of transitions in which hybrid aggregates go to amorphous aggregates that have two or more fewer chains.

The important points to take away from the specific transitions involving amorphous aggregates shown in Figure 6 are the following. Figures 6a and 6b show that after $t^* = 15$ it is more likely for a chain in an amorphous aggregate to transition into a hybrid aggregate of greater size than it is for the hybrid aggregate to collapse into a smaller-sized independent amorphous aggregate. Figures 6c and 6d show that before $t^* = 50$ it is twice as likely for an amorphous aggregate to rearrange into a beta sheet ($A \rightarrow B$ transition) than for a beta sheet to collapse into an amorphous aggregate (the corresponding $B \rightarrow A$ transition), but after $t^* = 50$ the percentage of those transitions equalizes, indicating the simulations have reached a steady state. The inequality in $A \rightarrow B$ and $B \rightarrow A$ transition probabilities between $t^* = 15$ and 50 leads to a decrease in the amorphous aggregate population and an increase in the beta sheet population due to the rearrangement of amorphous aggregates into beta sheets. From data not shown it is evident that after $t^* = 15$ the probability that an amorphous aggregate will decrease in size is the same as the probability that it will increase in size, indicating that these transitions do not contribute significantly to the increase or decreasing in the overall amorphous aggregate population.

Figure 7 shows the percentage of transitions that start from or end up in a hybrid aggregate including: the percentage of transitions that start from (a) amorphous aggregates, and (b) beta sheets or fibrils, and the percentage of transitions that result in (c) amorphous aggregates, and (d) beta sheets or fibrils as a function of time.

The important points to take away from the hybrid aggregate transitions shown in Figure 7 are the following. At very early times, before $t^* = 10$, hybrid aggregates are formed from a combination of amorphous aggregate rearrangement and monomer addition, as seen by the high percentage of $A \rightarrow H$ transitions in Figure 7a and from data not shown on $M \rightarrow H$. At longer times, $t^* > 50$, comparison of Figures 7b and 7d shows that fibril rearrangement occurs, with chains fluctuating back and forth between fibrils and hybrid aggregates in an attempt to minimize system free energy. The hybrid aggregate population does not change significantly by either the growth or reduction in size of the hybrid aggregates themselves since the percentages of forward and reverse transitions between hybrid aggregates of each size is approximately equal at all time points (data not shown). The number of hybrid aggregates decreases significantly by the time $t^* = 50$ as their unstructured chains rearrange into beta sheet conformations (all $H \rightarrow B$ transitions). This can be seen by comparing the percentages of $H \rightarrow B$ and $B \rightarrow H$ transitions in Figures 7b and 7d.

Figure 8 shows the percentage of transitions that start from or end up in a beta sheet including: the percentage of transitions that start from (a) free monomer or fibril, (b) amorphous aggregates, and (c) hybrid aggregates, and the percentage of transitions that end up in (d) free monomer or fibril, (e) amorphous aggregates, and (f) hybrid aggregates. The subscripts sm, eq, and lg on the F indicate that the chain came from a beta sheet in a fibril that was smaller, equal in size, or larger than the resulting amorphous aggregate, hybrid aggregate, or beta sheet. F_2 refers to a fibril with two sheets while F_p represents the population of fibrils containing more than two sheets. Different sets of observables are used to describe the transitions to a fibril and the transitions from a fibril because we want to answer different questions in each case. For transitions in the forward direction, we want to know how the first small fibrils form – specifically what aggregates stack together to form a two-sheet fibril. This is why the distinction between two-sheet fibrils and all other fibrils was made. For transitions in the backward direction we want to know how a fibril breaks apart, specifically where the separation occurs within the fibril. This led to the three

different fibril categories (sm, eq, lg) respectively indicating whether a fibril loses more than a single beta sheet, a complete beta sheet, or only a part of a single beta sheet.

The important points to take away from the various types of transitions involving beta sheets shown in Figure 8 are the following. Figures 8a and 8d show that at early times it is possible for beta sheets to grow by monomer addition and for two-chain beta sheets (B_2) to break apart into free monomers. At early times, before $t^* = 15$, amorphous aggregates rearrange into beta sheets, as indicated by the fact that the percentage of transitions from amorphous aggregates to beta sheets in Figure 8b is larger than the percentage of transitions from beta sheets to amorphous aggregates in Figure 8e (e.g. compare curves $A_k \rightarrow B_k$ with $B_k \rightarrow A_k$). Beta sheets are formed primarily from the reordering of amorphous aggregates of the same size or larger, as indicated by the large percentage of these types of transitions in Figure 8b. Not shown is data that indicates that free monomers rarely come together to form a dimer (B_2) (B_2 forms instead by the rearrangement of small amorphous aggregates) although subsequent growth of already formed beta sheets seems to be predominantly driven by monomer addition. The growth of beta sheets by the addition of multiple chains does occur, although not at as high a percentage as growth by a single chain. Figures 8e and 8f show that at early times ($t^* < 15$) the beta sheets are slightly unstable and likely to collapse into a hybrid aggregate or amorphous aggregate, they becomes less likely to collapse into amorphous aggregates or hybrid aggregates at later times. After $t^* = 15$ there is a slightly higher percentage of transitions from hybrid aggregates to beta sheets than from beta sheets to hybrid aggregates (cf. Figs. 8c and 8f). This indicates that hybrid aggregates are not forming new beta sheets. Instead the amorphous chains within the hybrid aggregates are slowly rearranging into beta sheet conformations. In Figure 8d, it is clear that at early times a beta sheet is likely to associate into a two sheet fibril, but once larger fibrils are present ($t^* > 40$) beta sheets are much more likely to add on to an existing fibril than to form a new fibril. Figure 8a shows that if a beta sheet is going to dissociate from a fibril, it is much more likely that a single sheet will dissociate from the fibril creating an equal size independent beta sheet, rather than a partial sheet dissociating to form a smaller beta sheet or multiple sheets dissociating to form a larger beta sheet. These beta-sheet-to-fibril and fibril-to-beta-sheet transitions occur most frequently at the end of the simulation, which is expected since that is when the large fibrils are rearranging in order to minimize the total free energy of the system.

Figure 9 shows the percentage of transitions that start from or end up in a fibril including: the percentage of transitions that start from (a) less ordered structures, and the percentage of transitions that end up in (b) a beta sheet or a hybrid aggregate. The sm, eq, and lg subscripts in Figure 9 have the same definitions as in Figure 8.

The important points to take away from Figure 9 and the specific transitions involving fibrils are the following. Two-sheet fibrils (F_2) form initially from beta sheet association and rearrangement of amorphous or hybrid aggregates as indicated in Figure 9a, which suggests that amorphous aggregate structure can be influenced by the presence of neighboring beta sheets, much like templated assembly. During the time when the percentage of peptide chains in a fibril is increasing rapidly ($t^* = 30$ to $t^* = 60$), growth occurs both by the addition of a single sheet and by the addition of multiple sheets (data not shown). During the early stages of fibril formation, a large percentage of the transitions from fibrils are to either beta sheets or hybrid aggregates as seen in Figure 9b; these dissociation transitions primarily include the loss of a whole beta sheet or the loss of more than one beta sheet as seen in Figure 9b. As the simulation progresses ($t^* > 40$) and most of the chains are in the fibril state, (see Figure 4a), the dissociation of chains from a fibril decreases significantly and the fibrils begin to rearrange. After about $t^* = 60$, the percentage of transitions indicating fibril growth by single sheet addition ($F_{p-1} \rightarrow F_p$) is matched by the percentage of transitions

involving fibril shrinkage by single sheet loss ($F_{p+1} \rightarrow F_p$) (data not shown); this indicates that the large fibril is formed and that the beta sheets within the fibril are rearranging to find the most stable and energetically favorable conformation.

In this paper the only fibril transitions considered are those where the total number of sheets in the fibril changes. These include the growth of a fibril by adding sheets or small fibrils, the dissociation of a fibril by loss of a beta sheet or small fibril, or the rearrangement of a fibril in which the total number of chains in the fibril remains constant but the number of sheets changes. There are other possibilities for fibril transitions that are not considered here. These include transitions in which the total number of sheets in a fibril does not change but the total number of chains does (*e.g.* growth of a beta sheet in a fibril). As stated previously, fibril rearrangement is not a focus of this paper, which is why those transitions are not shown in Figure 9. Free monomers do get added to an existing fibril, however this transition is a very small percentage when compared to the percentage of other fibril transitions and so is not included in Figure 9a since it would not change the number of beta sheets in the fibril.

Discussion

The behavior of the free monomers over the course of the simulation is not unexpected; they associate into small amorphous aggregates at very early stages ($t^* < 15$), add to these amorphous aggregates when the latter exist in substantial numbers ($15 < t^* < 30$), add to beta sheets when those structures are present in the simulation ($t^* > 15$), and add to fibrils once they appear in the simulation ($t^* > 30$). The only method the system has of replenishing the population of free monomers is the dissociation of amorphous or hybrid aggregates since it is not energetically favorable at this simulation temperature for monomers to dissociate from existing beta sheets or fibrils.

Beta sheets form from the restructuring of amorphous aggregates and mostly grow by the addition of a monomer or rearrangement of a hybrid aggregate; their numbers are depleted by the formation and growth of fibrils. Fibrils grow by the association of beta sheets and amorphous aggregates to form small fibrils; these then combine together and grow by adding newly forming beta sheets or adding reorganizing hybrid aggregates, until the vast majority of the peptides are incorporated into the large final structure. Once the majority of the peptide chains are in a fibril structure ($t^* > 60$) the number of sheets in the large fibril shows no net change since the percentage of transitions that add to the fibril equals the percentage of transitions that shrink the fibril. However, the total number of chains in the fibril grows by the addition of monomers or rearrangement of existing beta sheets and hybrid aggregates until the final structure is formed.

Amorphous aggregates form from the association of two free monomers and then quickly grow ($t^* < 15$). Once they are large enough (usually four or more chains), these amorphous aggregates then restructure into beta sheets ($15 < t^* < 50$). Since the transitions involving the growth and shrinking of amorphous aggregates occur during the beginning of the simulation, this indicates that the amorphous aggregates are unstable and not energetically favorable since they break apart as easily as they form. At the end of the simulation, there are no independent amorphous aggregates, instead unstructured chains associate with more ordered structures as part of hybrid aggregates which serve as intermediates during the fibril rearrangement process. The peptide chains classified as hybrid aggregates are continuously adopting and losing the cross-beta structure of the ordered part of the hybrid within the large fibrils in an attempt to minimize the system free energy. When these chains are not part of a beta sheet, they are counted as being part of a large hybrid aggregate because they do not completely dissociate from the fibril structure. Rather, for a brief period of time, the hybrid

chains are interacting with the fibril until they re-adopt the cross-beta structure and become part of the large fibril once more.

It is of interest to compare the percent of amorphous aggregates restructuring into beta sheets with the percent of beta sheets collapsing into amorphous aggregates since the most toxic species in the fibril formation pathway is known to be an intermediate oligomer with little or no cross-beta structure.^{11–18, 73} We have found that the amorphous aggregates restructure into beta sheets about twice as often as the beta sheets collapse into amorphous aggregates. The beta sheets that are formed are almost always the same size or smaller than the original amorphous aggregates, meaning that most times when a beta sheet is created along the fibril formation pathway, a smaller amorphous or hybrid aggregate remains in the system to grow and interact with other structures. There is no other way to create beta sheets in these simulations. This leads to the conclusion that the amorphous aggregates are necessary intermediates in the fibril formation pathway and that the restructuring of amorphous aggregates into beta sheets plays a key role in the fibrillization mechanism. The small beta sheets that are formed from the rearrangement of the amorphous aggregates are themselves unstable due to the exposed hydrophobic side chains. They therefore quickly associate into small fibril structures that continue to grow over the course of the simulations until the final structure resembles protofilaments. The small independent amorphous aggregates that form early in the simulation are energetically unfavorable at this simulation temperature, as evidenced by their depletion as the simulation progresses. All of the unstructured peptide chains that remain at the end of the simulation are associated with the large fibril as part of a hybrid aggregate, and are most likely in the process of reorganizing into the cross-beta structure in order to reorganize and add to the fibril.

The results presented in this paper are consistent with previous work published in the literature. Serio *et al.* found experimentally that the prion Sup35 monomers collapse into oligomers of varying size that resembled micellar-like structures, rearrange into more-ordered conformations and then proceed along the fibril formation pathway.⁵⁷ Necula *et al.* determined that in the presence of methylene blue, A β _{1–42} is forced to aggregate into small oligomers containing β -sheet content that eventually form fibrils.²² Using ProFASi atomistic Monte Carlo computer simulations Cheon *et al.* found that different lengths of A β peptides aggregate along different paths, with monomers of the shorter sequence A β _{16–22} forming amorphous aggregates that slowly rearrange into β -sheets, while monomers of the longer sequence A β _{25–35} directly adopt the β -sheet conformations.⁶⁴ Auer *et al.* used Monte Carlo computer simulations of a tube model protein to introduce the idea of a condensation mechanism for generic protein sequences which includes two steps: first, the formation of large amorphous aggregates and second, the rearrangement of the amorphous aggregate into a more ordered structure that eventually leads to fibril formation.¹⁸ Pallito and Murphy used a mathematical model to describe A β ₄₀ fibril formation kinetics that included as the key step the formation of an unstructured oligomeric nucleus from denatured monomers that then forms protofilaments.¹⁹ Powers and Powers published a mathematical model that describes a nucleated polymerization mechanism for protein aggregation in which monomers first aggregate into small oligomers until a nucleus (of unspecified size) is formed, after which the nucleus grows into a fibril conformation.^{43, 42} Zhang and Muthukumar used lattice Monte Carlo simulations to study how the peptide concentration, temperature, and seed size affected the nucleation and formation pathway. Their nucleation step involved the stacking of beta sheets into a fibril. At certain conditions the Ostwald effect prevailed, meaning that large fibrils grow at the expense of small fibrils producing a small number of large fibrils as opposed to a large number of small fibrils.⁷⁴ Pellarin *et al.* performed Langevin dynamics simulations of a coarse-grained model that supported the idea of having multiple aggregation pathways to the final fibril state. They found that reducing the propensity of a peptide to form beta structures actually increases the heterogeneity of the intermediates

found in pre-fibrillar intermediates; this might increase the number of toxic species created during fibril formation.⁷⁵ These works are consistent with the results presented in this paper that a possible key step in the formation of fibrils during protein aggregation is the rearrangement of unstructured or amorphous aggregates into a more ordered conformation, which then leads to the formation of protofilaments and fibrils.

Summary and Conclusions

The fibrillization pathway for this system of 192 KA₁₄K chains at T* = 0.13 and c = 5mM has the following steps. Monomers form small amorphous aggregates which grow to intermediate size and then transform or dissociate into smaller beta sheets and hybrid aggregates which grow slowly. Some of the resulting beta sheets quickly form small fibrils which then combine with the remaining amorphous aggregates, hybrid aggregates, and small beta sheets to form larger fibrils. Small sections of the large fibrils dissociate and re-associate in an attempt to find the most energetically favorable configuration. Figure 10 shows a diagram of this aggregation pathway.

Our work provides a picture of the structural reorganization process that occurs within the oligomers and the association of high order oligomers, including the role of cooperativity. Initially the amorphous aggregates are small in size, containing only two or three peptide chains. These grow to intermediate size, generally between four and seven chains. These then transition into either smaller size beta sheets (containing two to four chains) or hybrid aggregates (containing two chains to seven or more chains). The beta sheets subsequently grow in size to between five and seven chains at the same time as they begin stacking into small fibrils. The first small two-sheet fibrils have less than ten chains but quickly grow; the final large fibrils have on the order of one hundred chains. This final size is determined by the total number of chains in the system, the fibrils would grow even larger if there were more chains in the system.

The small amorphous intermediates formed in this pathway are necessary steps in the fibrillization process, since the beta sheets do not form directly from free monomers but instead from the restructuring of amorphous aggregates. The dearth of independent amorphous aggregates at the end of the simulation indicates that under these conditions individual amorphous aggregates are not stable and are therefore not part of a separate reaction pathway that competes with the fibrillization pathway. If the small amorphous aggregates are the toxic intermediate species found in the fibril formation process, this on-pathway formation of amorphous aggregates means that it will be difficult to influence the toxic oligomers without affecting the overall fibril formation process for a polyalanine system.

It is of interest to ask which of the polymerization mechanisms (nucleated polymerization, nucleated conformational conversion, and templated assembly) traditionally used to describe amyloid formation can be used to explain simulations. Amyloid fibrillization at the temperature considered here is more complicated than the traditional polymerization mechanisms. Many different types of oligomers form, these merge and undergo structural rearrangement until a fibril nucleus is formed which then grows by monomer and multi-mer addition. Conformational conversion does not apply to our simulations since the monomers start in a random configuration and not in the native state. While our results are consistent with the formation of a nucleus that grows and rearranges into larger well-ordered structures, the nucleated polymerization and the templated assembly mechanisms are not really good fits because our simulations show that the formation and growth of both unstable and stable aggregates is not solely due to monomer addition. In a forthcoming paper on

polyalanine aggregation we examine the dependence of the kinetics on temperature and find that the templated assembly process seems more applicable at higher temperatures.

Acknowledgments

This work was supported by the National Institutes of Health, USA under grants GM56766 and EB006006.

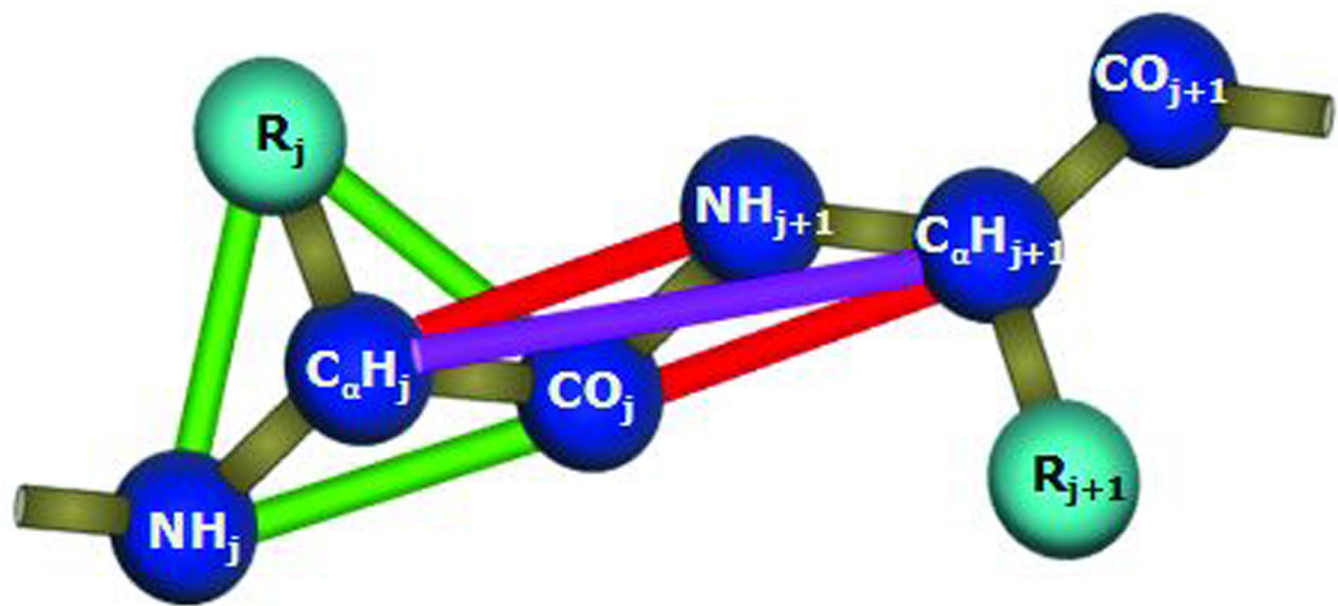
References Cited

1. Adamcik J, Jung JM, Flakowski J, De Los Rios P, Dietler G, Mezzenga R. Understanding amyloid aggregation by statistical analysis of atomic force microscopy images. *Nat Nanotechnol.* 2010 Jun; 5(6):423–428. [PubMed: 20383125]
2. Bieler S, Estrada L, Lagos R, Baeza M, Castilla J, Soto C. Amyloid formation modulates the biological activity of a bacterial protein. *Journal of Biological Chemistry.* 2005 Jul; 280(29):26880–26885. [PubMed: 15917245]
3. Bucciantini M, Giannoni E, Chiti F, Baroni F, Formigli L, Zurdo JS, Taddei N, Ramponi G, Dobson CM, Stefani M. Inherent toxicity of aggregates implies a common mechanism for protein misfolding diseases. *Nature.* 2002 Apr; 416(6880):507–511. [PubMed: 11932737]
4. Chiti F, Dobson CM. Protein misfolding, functional amyloid, and human disease. *Annual Review of Biochemistry.* 2006; 75:333–366.
5. Haass C, Selkoe DJ. Soluble protein oligomers in neurodegeneration: Lessons from the alzheimer's amyloid beta-peptide. *Nat Rev Mol Cell Biol.* 2007 Feb; 8(2):101–112. [PubMed: 17245412]
6. Kodali R, Wetzel R. Polymorphism in the intermediates and products of amyloid assembly. *Curr Opin Struct Biol.* 2007 Feb; 17(1):48–57. [PubMed: 17251001]
7. Lansbury PT, Lashuel HA. A century-old debate on protein aggregation and neurodegeneration enters the clinic. *Nature.* 2006 Oct; 443(7113):774–779. [PubMed: 17051203]
8. Nelson R, Sawaya MR, Balbirnie M, Madsen AO, Riek C, Grothe R, Eisenberg D. Structure of the cross-beta spine of amyloid-like fibrils. *Nature.* 2005 Jun; 435(7043):773–778. [PubMed: 15944695]
9. Petkova AT, Yau WM, Tycko R. Experimental constraints on quaternary structure in alzheimer's beta-amyloid fibrils. *Biochemistry.* 2006 Jan; 45(2):498–512. [PubMed: 16401079]
10. Serpell LC, Sunde M, Benson MD, Tennent GA, Pepys MB, Fraser PE. The protofilament substructure of amyloid fibrils. *Journal of Molecular Biology.* 2000 Jul; 300(5):1033–1039. [PubMed: 10903851]
11. Chiti F, Dobson CM. Amyloid formation by globular proteins under native conditions. *Nature Chemical Biology.* 2009 Jan; 5(1):15–22.
12. Gonzalez-Velasquez FJ, Kotarek JA, Moss MA. Soluble aggregates of the amyloid-beta protein selectively stimulate permeability in human brain microvascular endothelial monolayers. *Journal of Neurochemistry.* 2008 Oct; 107(2):466–477. [PubMed: 18702666]
13. Kayed R, Pensalfini A, Margol L, Sokolov Y, Sarsoza F, Head E, Hall J, Glabe C. Annular protofibrils are a structurally and functionally distinct type of amyloid oligomer. *Journal of Biological Chemistry.* 2009 Feb; 284(7):4230–4237. [PubMed: 19098006]
14. Kelly JW. Amyloid fibril formation and protein misassembly: A structural quest for insights into amyloid and prion diseases. *Structure.* 1997 May; 5(5):595–600. [PubMed: 9195890]
15. Ono K, Condron MM, Teplow DB. Structure-neurotoxicity relationships of amyloid beta-protein oligomers. *Proceedings of the National Academy of Sciences of the United States of America.* 2009 Sep; 106(35):14745–14750. [PubMed: 19706468]
16. Walsh DM, Selkoe DJ. A beta oligomers - a decade of discovery. *J Neurochem.* 2007 Jun; 101(5): 1172–1184. [PubMed: 17286590]
17. Auer S, Meersman F, Dobson CM, Vendruscolo M. A generic mechanism of emergence of amyloid protofilaments from disordered oligomeric aggregates. *PLoS Comput Biol.* 2008 Nov; 4(11)
18. Auer S, Dobson CM, Vendruscolo M. Characterization of the nucleation barriers for protein aggregation and amyloid formation. *Hfsp J.* 2007 Jul; 1(2):137–146. [PubMed: 19404419]

19. Pallitto MM, Murphy RM. A mathematical model of the kinetics of beta-amyloid fibril growth from the denatured state. *Biophysical Journal*. 2001 Sep; 81(3):1805–1822. [PubMed: 11509390]
20. Glabe CG. Structural classification of toxic amyloid oligomers. *Journal of Biological Chemistry*. 2008 Oct; 283(44):29639–29643. [PubMed: 18723507]
21. Rangachari V, Moore BD, Reed DK, Sonoda LK, Bridges AW, Conboy E, Hartigan D, Rosenberry TL. Amyloid-beta(1–42) rapidly forms protofibrils and oligomers by distinct pathways in low concentrations of sodium dodecylsulfate. *Biochemistry*. 2007 Oct; 46(43):12451–12462. [PubMed: 17910477]
22. Necula M, Breydo L, Milton S, Kayed R, van der Veer WE, Tone P, Glabe CG. Methylene blue inhibits amyloid A beta oligomerization by promoting fibrillization. *Biochemistry*. 2007 Jul; 46(30):8850–8860. [PubMed: 17595112]
23. Necula M, Kayed R, Milton S, Glabe CG. Small molecule inhibitors of aggregation indicate that amyloid beta oligomerization and fibrillization pathways are independent and distinct. *Journal of Biological Chemistry*. 2007 Apr; 282(14):10311–10324. [PubMed: 17284452]
24. Chebaro Y, Dong X, Laghaei R, Derreumaux P, Mousseau N. Replica exchange molecular dynamics simulations of coarse-grained proteins in implicit solvent. *J Phys Chem B*. 2009 Jan; 113(1):267–274. [PubMed: 19067549]
25. Derreumaux P, Mousseau N. Coarse-grained protein molecular dynamics simulations. *J Chem Phys*. 2007 Jan; 126(2)
26. Urbanc B, Betnel M, Cruz L, Bitan G, Teplow DB. Elucidation of amyloid beta-protein oligomerization mechanisms: Discrete molecular dynamics study. *Journal of the American Chemical Society*. 2010 Mar; 132(12):4266–4280. [PubMed: 20218566]
27. Wei GH, Song W, Derreumaux P, Mousseau N. Self-assembly of amyloid-forming peptides by molecular dynamics simulations. *Front Biosci*. 2008 May; 13:5681–5692. [PubMed: 18508615]
28. Marchut AJ, Hall CK. Spontaneous formation of annular structures observed in molecular dynamics simulations of polyglutamine peptides. *Computational Biology and Chemistry*. 2006 Jun; 30(3):215–218. [PubMed: 16678490]
29. Cellmer T, Douma R, Huebner A, Prausnitz J, Blanch H. Kinetic studies of protein L aggregation and disaggregation. *Biophysical Chemistry*. 2007 Feb; 125(2–3):350–359. [PubMed: 17055144]
30. Miller Y, Ma BY, Nussinov R. Synergistic interactions between repeats in tau protein and A beta amyloids may be responsible for accelerated aggregation via polymorphic states. *Biochemistry*. 2011 Jun; 50(23):5172–5181. [PubMed: 21506544]
31. Miller Y, Ma BY, Nussinov R. Polymorphism of alzheimer's A beta(17–42) (p3) oligomers: The importance of the turn location and its conformation. *Biophysical Journal*. 2009 Aug; 97(4):1168–1177. [PubMed: 19686665]
32. Straub, JE.; Thirumalai, D. Toward a molecular theory of early and late events in monomer to amyloid fibril formation. In: Leone, SR.; Cremer, PS.; Groves, JT.; Johnson, MA., editors. Annual review of physical chemistry. Vol. vol 62. Straub, John E. Thirumalai, D; 2011.
33. Straub JE, Thirumalai D. Principles governing oligomer formation in amyloidogenic peptides. *Current Opinion in Structural Biology*. 2010 Apr; 20(2):187–195. [PubMed: 20106655]
34. Tarus B, Straub JE, Thirumalai D. Probing the initial stage of aggregation of the A beta(10–35)-protein: Assessing the propensity for peptide dimerization. *Journal of Molecular Biology*. 2005 Feb; 345(5):1141–1156. [PubMed: 15644211]
35. Cerdá-Costa N, Esteras-Chopo A, Aviles FX, Serrano L, Villegas V. Early kinetics of amyloid fibril formation reveals conformational reorganisation of initial aggregates. *Journal of Molecular Biology*. 2007 Mar; 366(4):1351–1363. [PubMed: 17204287]
36. Chen SM, Ferrone FA, Wetzel R. Huntington's disease age-of-onset linked to polyglutamine aggregation nucleation. *Proceedings of the National Academy of Sciences of the United States of America*. 2002 Sep; 99(18):11884–11889. [PubMed: 12186976]
37. Bellesia G, Shea JE. Effect of beta-sheet propensity on peptide aggregation. *Journal of Chemical Physics*. 2009 Apr; 130(14)
38. Bellesia G, Shea JE. Diversity of kinetic pathways in amyloid fibril formation. *Journal of Chemical Physics*. 2009 Sep; 131(11)

39. Knowles TPJ, Waudby CA, Devlin GL, Cohen SIA, Aguzzi A, Vendruscolo M, Terentjev EM, Welland ME, Dobson CM. An analytical solution to the kinetics of breakable filament assembly. *Science*. 2009 Dec; 326(5959):1533–1537. [PubMed: 20007899]
40. Lee CC, Nayak A, Sethuraman A, Belfort G, McRae GJ. A three-stage kinetic model of amyloid fibrillation. *Biophysical Journal*. 2007 May; 92(10):3448–3458. [PubMed: 17325005]
41. Murphy RM. Kinetics of amyloid formation and membrane interaction with amyloidogenic proteins. *Biochimica Et Biophysica Acta-Biomembranes*. 2007 Aug; 1768(8):1923–1934.
42. Lomakin A, Teplow DB, Kirschner DA, Benedek GB. Kinetic theory of fibrillogenesis of amyloid beta-protein. *Proceedings of the National Academy of Sciences of the United States of America*. 1997 Jul; 94(15):7942–7947. [PubMed: 9223292]
43. Powers ET, Powers DL. The kinetics of nucleated polymerizations at high concentrations: Amyloid fibril formation near and above the "supercritical concentration". *Biophysical Journal*. 2006 Jul; 91(1):122–132. [PubMed: 16603497]
44. Roberts CJ, Darrington RT, Whitley MB. Irreversible aggregation of recombinant bovine granulocyte-colony stimulating factor (bG-CSF) and implications for predicting protein shelf life. *Journal of Pharmaceutical Sciences*. 2003 May; 92(5):1095–1111. [PubMed: 12712430]
45. Caughey B, Lansbury PT. Protofibrils, pores, fibrils, and neurodegeneration: Separating the responsible protein aggregates from the innocent bystanders. *Annual Review of Neuroscience*. 2003; 26:267–298.
46. Gibson TJ, Murphy RM. Inhibition of insulin fibrillogenesis with targeted peptides. *Protein Science*. 2006 May; 15(5):1133–1141. [PubMed: 16597825]
47. Bhattacharyya AM, Thakur AK, Wetzel R. Polyglutamine aggregation nucleation: Thermodynamics of a highly unfavorable protein folding reaction. *Proceedings of the National Academy of Sciences of the United States of America*. 2005 Oct; 102(43):15400–15405. [PubMed: 16230628]
48. Cannon MJ, Williams AD, Wetzel R, Myszka DG. Kinetic analysis of beta-amyloid fibril elongation. *Analytical Biochemistry*. 2004 May; 328(1):67–75. [PubMed: 15081909]
49. Kelly JW. Mechanisms of amyloidogenesis. *Nature Structural Biology*. 2000 Oct; 7(10):824–826.
50. Bernacki JP, Murphy RM. Model discrimination and mechanistic interpretation of kinetic data in protein aggregation studies. *Biophysical Journal*. 2009 Apr; 96(7):2871–2887. [PubMed: 19348769]
51. Davis TJ, Soto-Ortega DD, Kotarek JA, Gonzalez-Velasquez FJ, Sivakumar K, Wu LY, Wang Q, Moss MA. Comparative study of inhibition at multiple stages of amyloid-beta self-assembly provides mechanistic insight. *Molecular Pharmacology*. 2009 Aug; 76(2):405–413. [PubMed: 19483107]
52. Vitalis A, Lyle N, Pappu RV. Thermodynamics of beta-sheet formation in polyglutamine. *Biophysical Journal*. 2009 Jul; 97(1):303–311. [PubMed: 19580768]
53. Vitalis A, Wang XL, Pappu RV. Atomistic simulations of the effects of polyglutamine chain length and solvent quality on conformational equilibria and spontaneous homodimerization. *Journal of Molecular Biology*. 2008 Dec; 384(1):279–297. [PubMed: 18824003]
54. Williamson TE, Vitalis A, Crick SL, Pappu RV. Modulation of polyglutamine conformations and dimer formation by the N-terminus of huntingtin. *Journal of Molecular Biology*. 2010 Mar; 396(5):1295–1309. [PubMed: 20026071]
55. Krishnan R, Lindquist SL. Structural insights into a yeast prion illuminate nucleation and strain diversity. *Nature*. 2005 Jun; 435(7043):765–772. [PubMed: 15944694]
56. Mukhopadhyay S, Krishnan R, Lemke EA, Lindquist S, Deniz AA. A natively unfolded yeast prion monomer adopts an ensemble of collapsed and rapidly fluctuating structures. *Proc Natl Acad Sci U S A*. 2007 Feb; 104(8):2649–2654. [PubMed: 17299036]
57. Serio TR, Cashikar AG, Kowal AS, Sawicki GJ, Moslehi JJ, Serpell L, Arnsdorf MF, Lindquist SL. Nucleated conformational conversion and the replication of conformational information by a prion determinant. *Science*. 2000 Aug; 289(5483):1317–1321. [PubMed: 10958771]
58. Ding F, Dokholyan NV, Buldyrev SV, Stanley HE, Shakhnovich EI. Molecular dynamics simulation of the SH3 domain aggregation suggests a generic amyloidogenesis mechanism. *Journal of Molecular Biology*. 2002 Dec; 324(4):851–887. [PubMed: 12460582]

59. Blondelle SE, Forood B, Houghten RA, PerezPaya E. Polyalanine-based peptides as models for self-associated beta-pleated-sheet complexes. *Biochemistry*. 1997 Jul; 36(27):8393–8400. [PubMed: 9204887]
60. Nguyen HD, Hall CK. Molecular dynamics simulations of spontaneous fibril formation by random-coil peptides. *Proceedings of the National Academy of Sciences of the United States of America*. 2004 Nov; 101(46):16180–16185. [PubMed: 15534217]
61. Nguyen HD, Hall CK. Phase diagrams describing fibrillization by polyalanine peptides. *Biophysical Journal*. 2004 Dec; 87(6):4122–4134. [PubMed: 15465859]
62. Nguyen HD, Hall CK. Kinetics of fibril formation by polyalanine peptides. *Journal of Biological Chemistry*. 2005 Mar; 280(10):9074–9082. [PubMed: 15591317]
63. Nguyen HD, Hall CK. Spontaneous fibril formation by polyalanines; discontinuous molecular dynamics simulations. *Journal of the American Chemical Society*. 2006 Feb; 128(6):1890–1901. [PubMed: 16464090]
64. Cheon M, Chang I, Mohanty S, Luheshi LM, Dobson CM, Vendruscolo M, Favrin G. Structural reorganisation and potential toxicity of oligomeric species formed during the assembly of amyloid fibrils. *PLoS Comput Biol*. 2007 Sep; 3(9):1727–1738. [PubMed: 17941703]
65. Smith AV, Hall CK. Alpha-helix formation: Discontinuous molecular dynamics on an intermediate-resolution protein model. *Proteins-Structure Function and Genetics*. 2001 Aug; 44(3): 344–360.
66. Smith AV, Hall CK. Assembly of a tetrameric alpha-helical bundle: Computer simulations on an intermediate-resolution protein model. *Proteins-Structure Function and Genetics*. 2001 Aug; 44(3): 376–391.
67. Nguyen HD, Marchut AJ, Hall CK. Solvent effects on the conformational transition of a model polyalanine peptide. *Protein Science*. 2004 Nov; 13(11):2909–2924. [PubMed: 15498937]
68. Smith SW, Hall CK, Freeman BD. Molecular dynamics for polymeric fluids using discontinuous potentials. *J Comput Phys*. 1997 Jun; 134(1):16–30.
69. Alder BJ, Wainwright TE. STUDIES IN MOLECULAR DYNAMICS.1. GENERAL METHOD. *Journal of Chemical Physics*. 1959; 31(2):459–466.
70. Rapaport DC. MOLECULAR-DYNAMICS STUDY OF A POLYMER-CHAIN IN SOLUTION. *Journal of Chemical Physics*. 1979; 71(8):3299–3303.
71. Rapaport DC. MOLECULAR-DYNAMICS SIMULATION OF POLYMER-CHAINS WITH EXCLUDED VOLUME. *Journal of Physics a-Mathematical and General*. 1978; 11(8):L213–L217.
72. Andersen HC. MOLECULAR-DYNAMICS SIMULATIONS AT CONSTANT PRESSURE AND/OR TEMPERATURE. *Journal of Chemical Physics*. 1980; 72(4):2384–2393.
73. Lee CC, Walters RH, Murphy RM. Reconsidering the mechanism of polyglutamine peptide aggregation. *Biochemistry*. 2007 Nov; 46(44):12810–12820. [PubMed: 17929830]
74. Zhang JN, Muthukumar M. Simulations of nucleation and elongation of amyloid fibrils. *Journal of Chemical Physics*. 2009 Jan; 130(3)
75. Pellarin R, Guarnera E, Caflisch A. Pathways and intermediates of amyloid fibril formation. *J Mol Biol*. 2007 Dec; 374(4):917–924. [PubMed: 18028943]

**Figure 1.**

Geometric representation of polyalanine in PRIME showing backbone united atoms (dark blue), alanine side chain (light blue), covalent bonds (brown), and pseudo-bonds that maintain L-isomerization (green), realistic backbone angles (red) and the *trans* conformation (purple). Atoms are not shown to scale for ease of viewing.

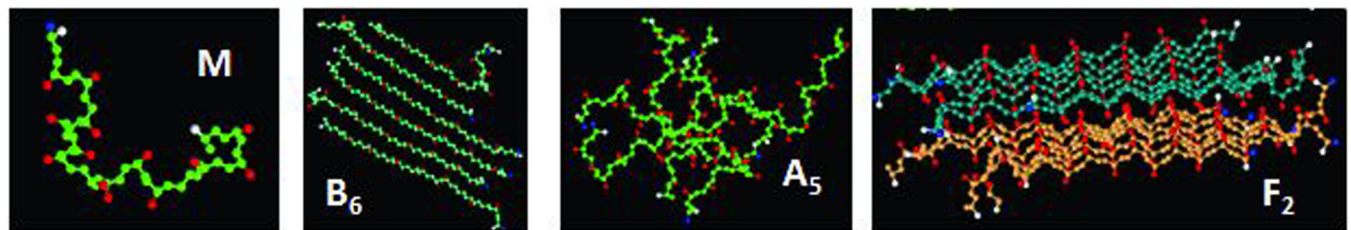


Figure 2.

Representation of various structures – M is a free monomer, B₆ is a beta sheet with six peptide chains, A₅ is an amorphous aggregate consisting of five peptide chains, and F₂ is a fibril that contains two beta sheets.

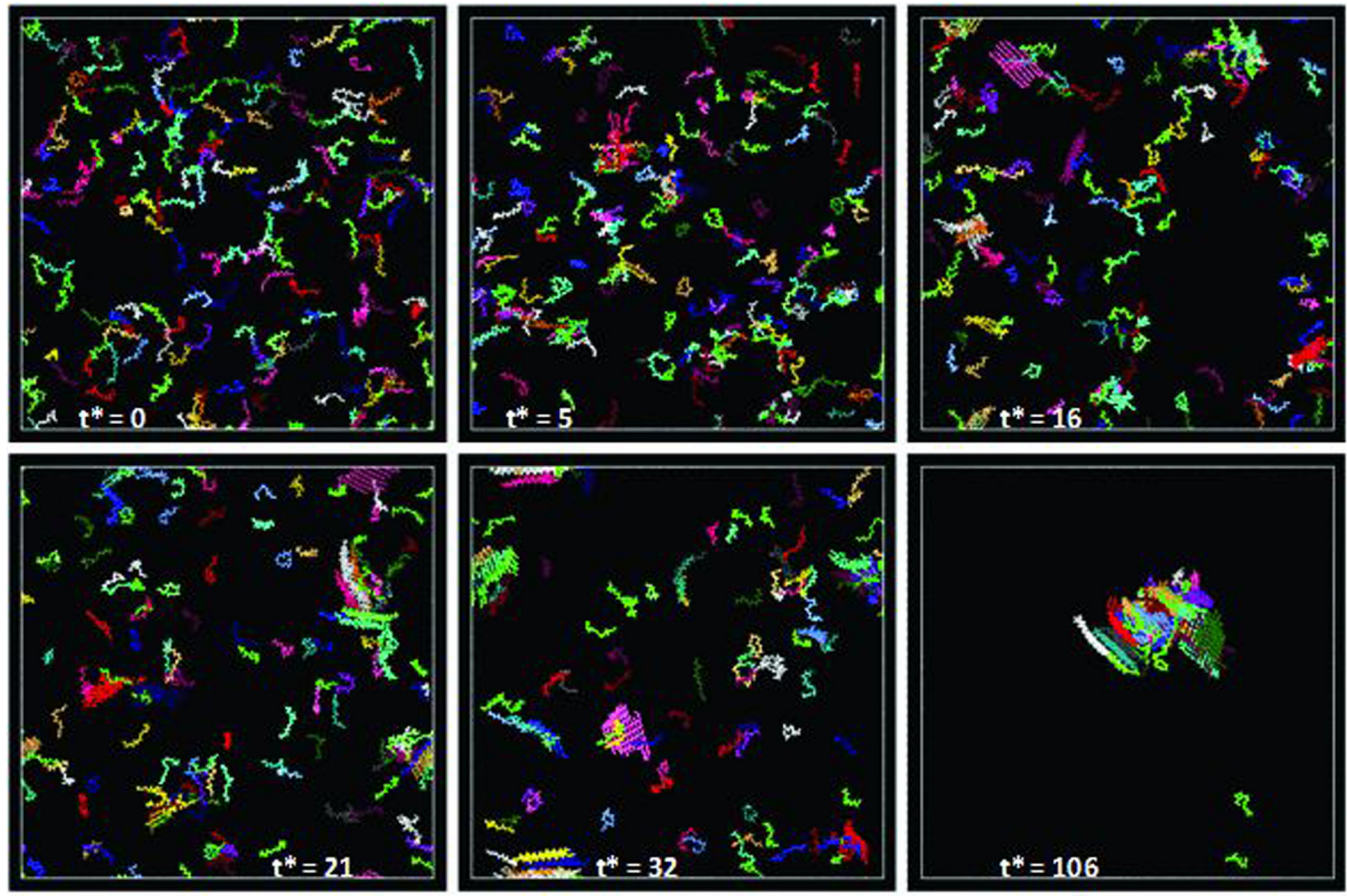
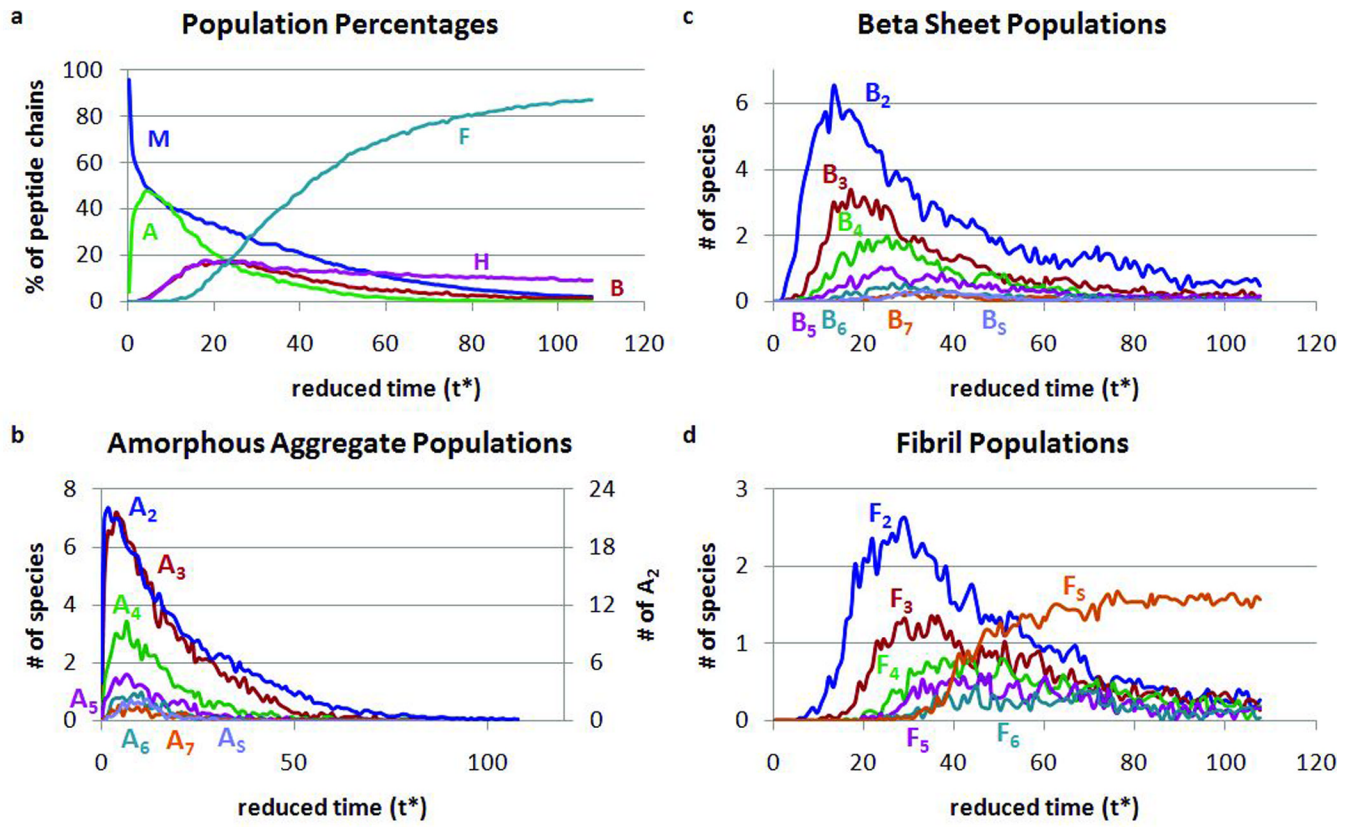
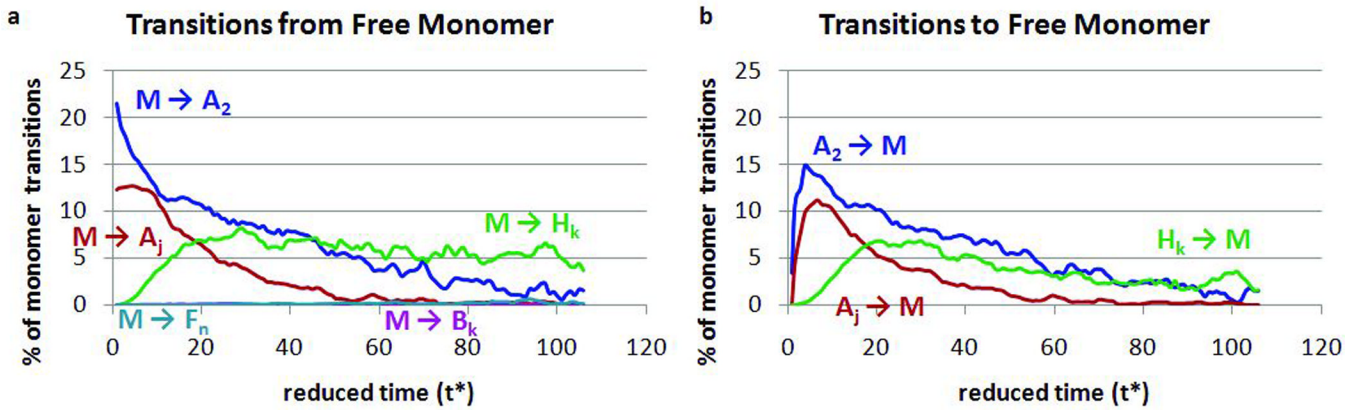


Figure 3.

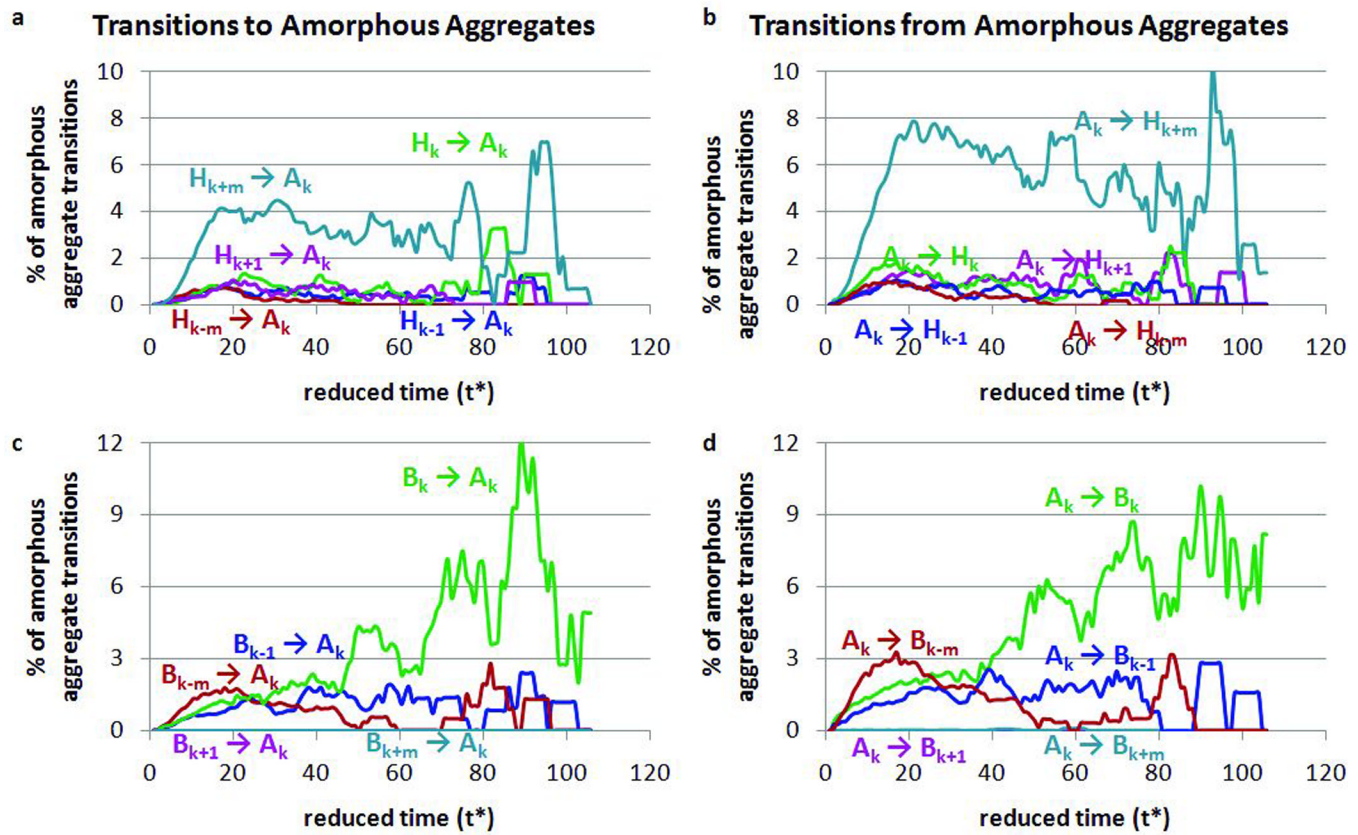
Snapshots taken over the course of one simulation at $T^* = 0.13$ and $c = 5\text{mM}$. Peptide chains are colored according to their final conformation so that all chains in the same beta sheet at the end of the simulation are the same color; amorphous and free monomer chains are bright green.

**Figure 4.**

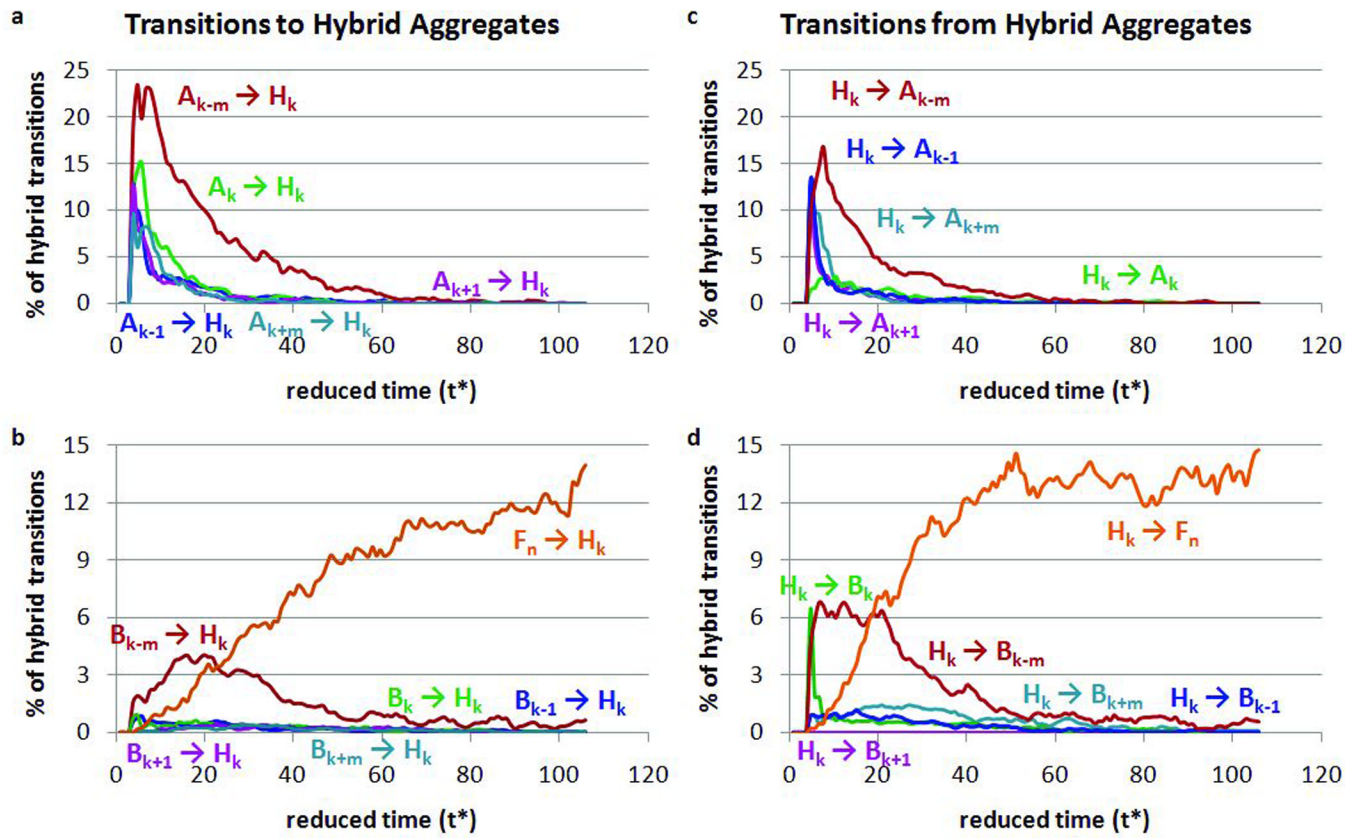
Populations of structures versus time. (a) percentage of peptide chains in each structure, (b) number of amorphous aggregates of each size, (c) number of beta sheets of each size, and (d) number of fibrils of each size.

**Figure 5.**

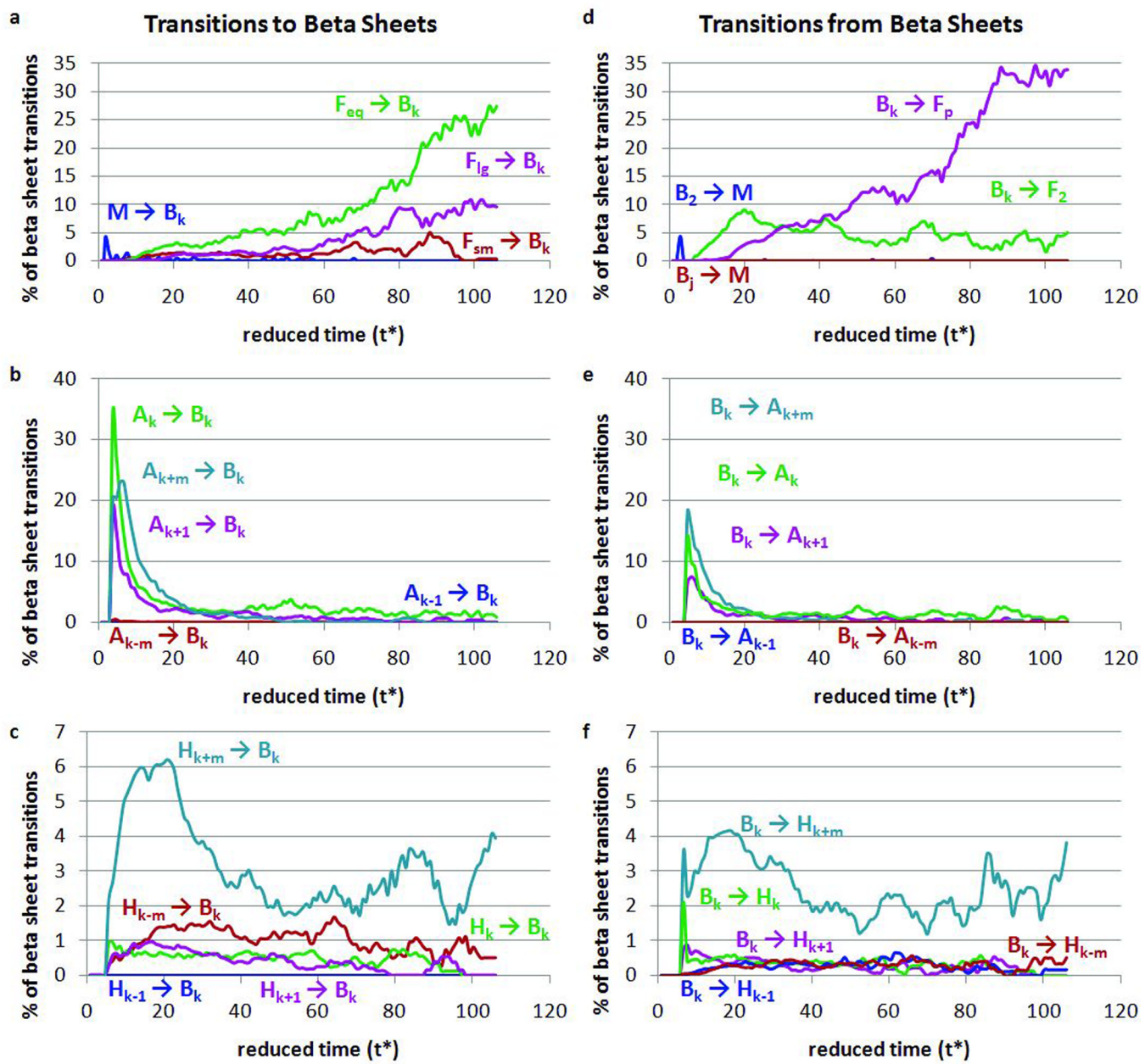
The percentage of chains that (a) start as a free monomer and transition to a different structure, and (b) start in a different structure and transition to a free monomer as a function of time.

**Figure 6.**

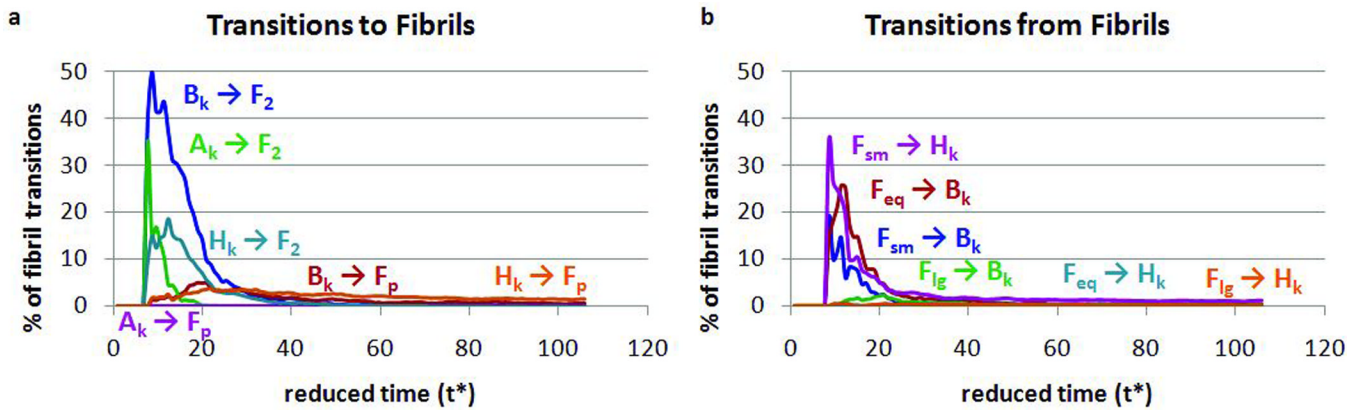
Amorphous aggregate transitions versus time. Left: percentage of chains that transition to amorphous aggregates from (a) hybrid aggregates, and (c) beta sheets. Right: percentage of chains that transition from an amorphous aggregate to (b) hybrid aggregates, and (d) beta sheets.

**Figure 7.**

Hybrid aggregate transitions versus time. Left: percentage of chains that transition to hybrid aggregates from (a) amorphous aggregates, and (b) beta sheets or fibrils. Right: percentage of chains that transition from a hybrid aggregate to (c) amorphous aggregates, and (d) beta sheets or fibrils.

**Figure 8.**

Beta sheet transitions versus time. Left: percentage of chains that transition to beta sheets from (a) free monomers and fibrils, (b) amorphous aggregates, and (c) hybrid aggregates. Right: percentage of chains that transition from beta sheets to (d) free monomers and fibrils, (e) amorphous aggregates, and (f) hybrid aggregates.

**Figure 9.**

Fibril Transitions versus time. Left: percentage of chains that transition to a fibril from (a) beta sheets, hybrid aggregates, and amorphous aggregates. Right: percentage of chains that transition from a fibril to (b) beta sheets or hybrid aggregates.

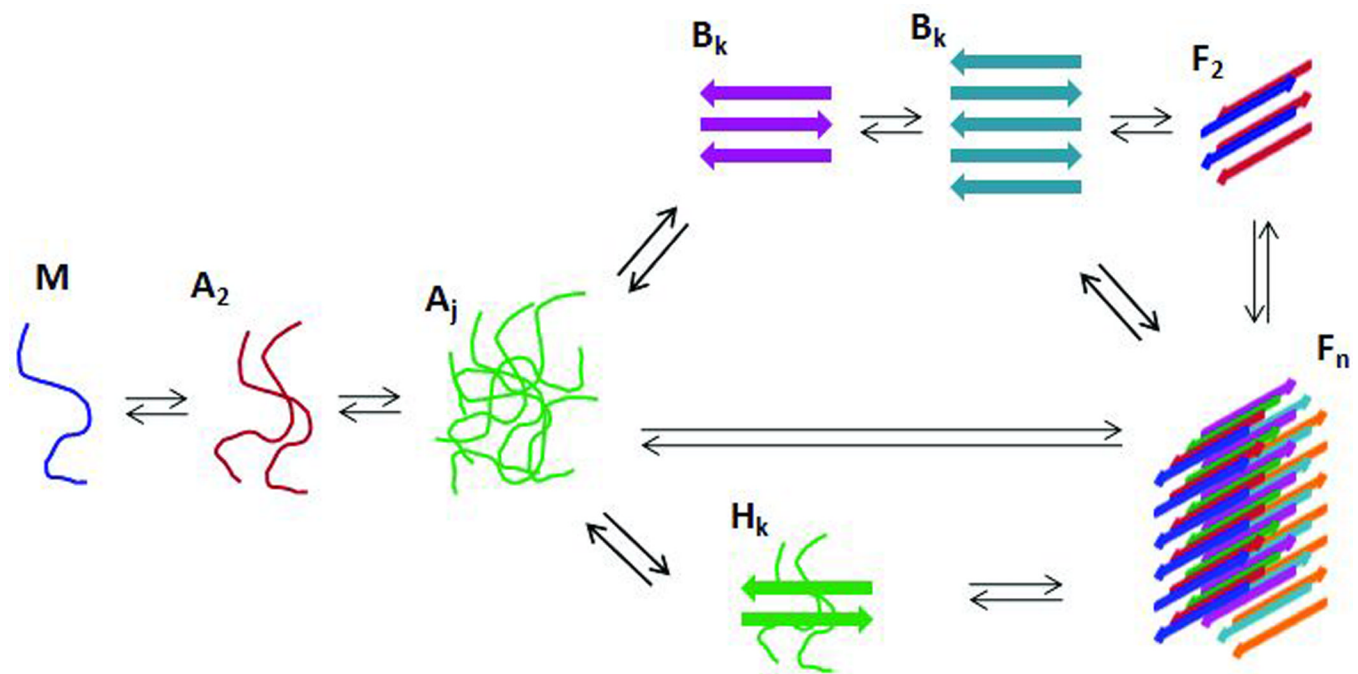
**Figure 10.**

Diagram of the aggregation pathway. Free monomers associate into small amorphous aggregates which grow and then rearrange into beta sheets and hybrid aggregates. The beta sheets grow and associate together to form two-sheet fibrils. The small fibrils grow by the addition of other beta sheets, amorphous aggregates, and hybrid aggregates to form large fibril structures.